Forside

Eksamensinformation
NFYB05035E - Bachelor Project in Physics, Niels Bohr Institute - Group Project

Besvarelsen afleveres af
Christine Pløger Lauritzen
qwz357@alumni.ku.dk

Niels Anders Lyngsø Bærentzen
rjn173@alumni.ku.dk

Eksamensadministratorer
Eksamensteam, tel 35 33 64 57
eksamen@science.ku.dk

Bedømmere
Kim Lefmann
Eksaminator
lefmann@nbi.ku.dk

Jørn Bindslev Hansen
Censor
jbh@fysik.dtu.dk

Besvarelsesinformationer

Titel: High Entropy LSCO - Synthesis & Testing: Introducing High Entropy to the LSCO superconductor
Titel, engelsk: High Entropy LSCO - Synthesis & Testing: Introducing High Entropy to the LSCO superconductor
Tro og love-erklæring: Ja

High Entropy LSCO - Synthesis & Testing

Introducing High Entropy to the LSCO superconductor

Bachelor Thesis

Written by *Christine Pløger Lauritzen & N. Anders L. Bærentzen*

June 16, 2023

Supervised by
Kim Lefmann & Andrea Kirsch

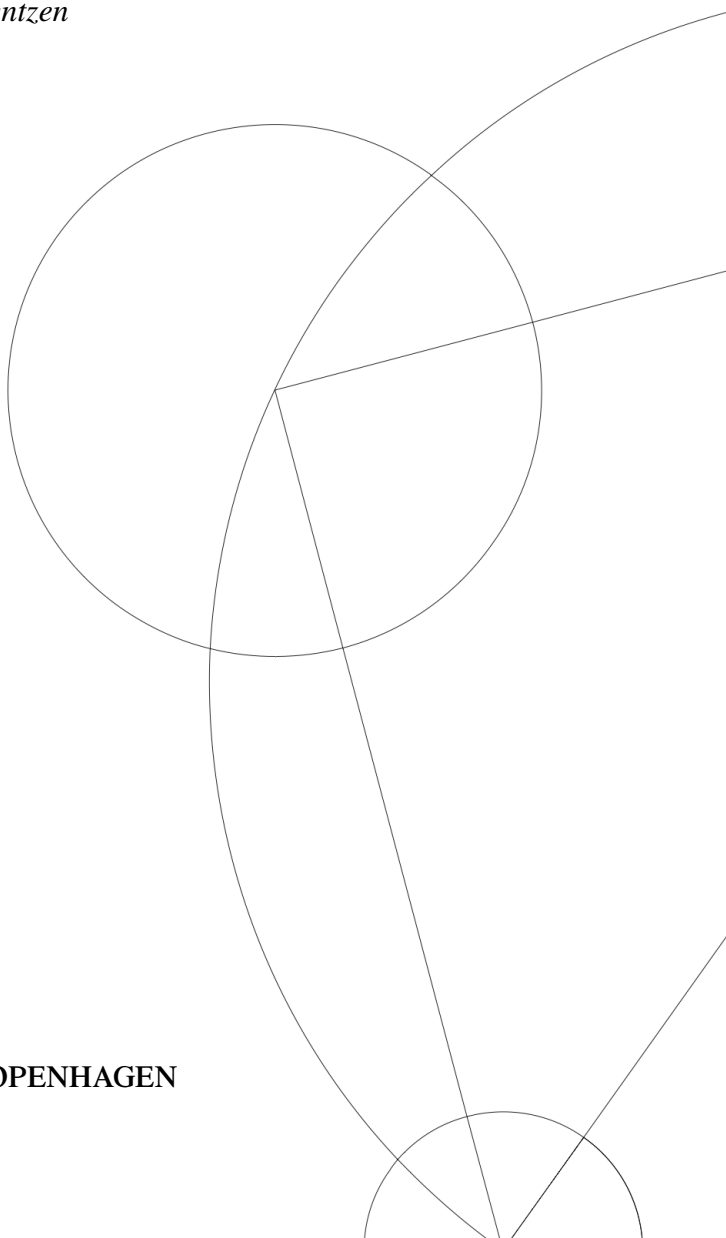

University of Copenhagen

UNIVERSITY OF
COPENHAGEN

Name of Institute:	Niels Bohr Institute
Name of Department:	Condensed Matter Physics
Author(s):	Christine Pløger Lauritzen & N. Anders L. Bærentzen
Email:	rjn173@alumni.ku.dk & qwz357@alumni.ku.dk
Title and subtitle:	High Entropy LSCO - Synthesis & Testing - Introducing High Entropy to the LSCO superconductor
Supervisor(s):	Kim Lefmann & Andrea Kirsch
Handed in:	16.06.2023
Defended:	20.06.2023

Name _____ Name _____

Signature _____ Signature _____

Date _____ Date _____

Abstract

In this thesis we aim to synthesise and characterise high entropy oxides based on the known superconductor $La_{1.85}Sr_{0.15}CuO_4$ (LSCO). The LSCO is made high entropic by doping the rare earth elements Nd, Eu and Sm into LSCO replacing the lanthanum. Four samples, each increasing in the amount of different rare earths doped in: no doping, Nd, Nd and Eu, and Nd, Eu and Sm respectively. The samples are made using the Sol-Gel method and their structures are analysed using powder X-ray diffraction (PXRD). The PXRD-data is then refined and show that LSCO was successfully made, while the other samples are in two or more phases. The analysis show that some of the samples crystallised both into the spacegroup *I4/mmm* and the lower symmetry spacegroup *Bmab*. Then susceptibility is measured on all the samples using a MPMS3 SQUID. Both Field Cooled and Zero Field Cooled measurements where taken at multiple field strengths for all samples. The results show that LSCO is superconducting with a critical temperature of 37.3 K, while the other three samples show paramagnetic behaviour.

Acknowledgements

We would like to thank all the people who have helped us with this project. First of all we would like to thank our supervisor Kim Lefmann for the great opportunity it has been to work on this project and for his invaluable inputs. We would also like to thank our other supervisor Andrea Kirsch for her invaluable help with the actual synthesis, for helping us do the X-ray diffraction and for sharing all her knowledge about high entropy materials and crystal structures.
We also wish to thank Kristine M. L. Krighaar for being there with us through the entire process and and answering all of our questions about basically anything.
We also want to extent our thanks to Bo Brummerstedt Iversen's group from Aarhus University for allowing us to use their SQUID and a special thanks to Vijay Singh Parmar and Hannah Hedegaard Nielsen for the instructions in how to use the SQUID and their help planning and taking the susceptibility measurements.
Thanks to Henrik Jacobsen and Thomas S. Christensen for sharing data and expertise with us for the discussion.
Thanks also to Asbjørn F. Lyngholm Preuss for great and insightful input to the thesis.
We would also like to thank everyone in the X-ray and Neutron science group for their support and insights into the world of condensed matter physics.
Finally we would like to thank Mark Cloos Videbæk for help with taking some of our X-ray diffraction measurements and Bastian Holten-Møller for assistance during one of the X-ray diffraction experiments.

Contents

1 Introduction

Superconductors were first discovered more than 100 years ago and since then more and more new materials have been found to be superconducting. The first high temperature superconductor was found in 1986 and was the cuprate $La_{2-x}Ba_xCuO_4$ (1). Since then there have been many new discoveries in the realm of high temperature superconductors, but also specifically for the family cuprates. Many cuperates were found to be superconducting and have some of the highest critical temperatures such as HgBaCaCuO which become superconducting at 135 K (2). These high transition temperatures means that a lot of research is going into both studying known superconducting cuprates and finding new methods for producing high temperature superconducting cuprates. Despite the extensive research done on the topic no consensus has been reached about how they work.

Another relatively new field in material science is the development of high entropy materials. High entropy materials or High Entropy Alloys (HEA) were first made in 2004 and refer to materials with at least 5 metallic elements, each with an atomic percentage of 5-35%. It has been known for a long time that addition of extra elements can change the properties of a material for example if carbon is added to iron, then the harder material, steel, is achieved. While steel is not a high entropy material, HEAs are a new way to explore how adding different elements change the properties of materials. So there is a lot of interest in researching these new materials (3). An even more recent discovery was the synthesis of high entropy cuprate $(La_{0.2}Pr_{0.2}Nd_{0.2}Sm_{0.2}Er_{0.2})_2CuO_4$ with the same structure type, *I4/mmm*, as the superconducting $La_{2-x}Sr_xCuO_4$, however without it being superconducting (4).

In 2014 the HEA Ti-Zr-Nb-Hf-Ta was found to be superconducting and in recent years research have gone into exploring the possibility of finding other high entropy superconducting materials (5). The spirit of this project is to follow in that track and try making new high entropy materials that might be superconducting.

In this thesis we will focus on trying to make high entropy cuprates which structure look like a known superconductor. We aim to see if the same method for making these high entropy cuprates can be used to synthesise the known superconductor LSCO. In addition we will also try to create new rare earth doped versions of LSCO and a new high entropy cuprate, by doping LSCO with one to three other lanthanides, while keeping the strontium doping the same. As far as we can find in literature these exact materials have not been synthesised before. We will characterise these new materials by doing powder X-ray diffraction and measuring the susceptibility with a SQUID.
The goal of this project is to find out what effect doping with several lanthanides, and thereby introducing more entropy, has on the superconductive properties of the LSCO superconductor.

2 Superconductivity

In this section we present an introduction to the properties of both superconductors in general, the current theory of low temperature superconductors and a short overview of high temperature cuprate superconductors.

Superconductivity is the phenomenon of a material losing all resistivity below a certain temperature called the critical temperature or T_c. At T_c the material undergoes a phase transition from

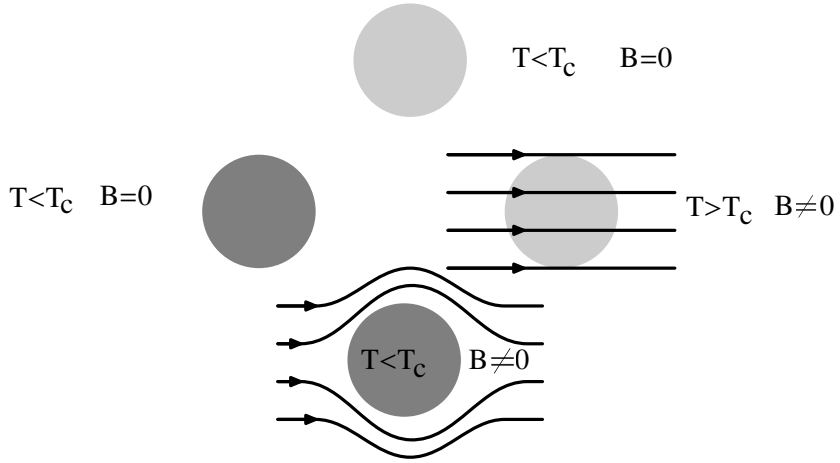

Figure 1: The two parts of the Meissner-Ochsenfeld effect illustrated, adapted from (6).

a normal state to a superconducting state (6). The first superconductor was discovered in 1911 by Kammerlingh Onnes when he used liquid helium to cool pure mercury to 4.18 K and found that the resistivity of the sample dropped abruptly to zero (7). Since then many other elements like aluminium and lead were found to be superconducting at temperatures typically below 10 K (8).

2.1 Meissner-Ochsenfeld effect

One of the important properties of a superconductor is that it expels weak magnetic fields (6). This effect was first discovered by Walther Meissner and Robert Ochsenfeld in 1933 (9) and is now one of the defining criteria for a superconductor. The effect can partially be explained as a consequence of zero resistivity, but not completely. Drude theory of conductivity gives the following connection between the electric field and the current for a conductor (6).

$$\mathbf{E} = \rho \cdot \mathbf{j} \tag{1}$$

With $\rho = 0$ in a superconductor the electric field must be zero. That combined with Maxwell's equations means that $\frac{\partial \mathbf{B}}{\partial t} = 0$. Or said another way, the magnetic field inside a superconductor that has been cooled below T_c cannot change. If there was no magnetic field applied before it was cooled, then no magnetic field can be created inside the superconductor (6). This happens because the superconductor when subjected to a magnetic field creates surface currents that in turn creates an opposite magnetic field that completely cancels out the applied field. According to Maxwell's equations for electromagnetic fields in a magnetic medium this means that the susceptibility has to be $\chi = -1$ when the superconductor is cooled below T_c. Which gives the following equality.

$$\mathbf{M} = -\mathbf{H} \tag{2}$$

An illustration of the effect can be seen in figure 1. A superconductor that is in a magnetic field and then cooled below the critical temperature will also expel the magnetic field in the same way. This effect cannot be explained only as a consequence of zero resistivity and is considered a separate phenomenon. Both effects together is called the Meissner-Ochsenfeld effect (6).

2.2 Type I and II

For superconductors to behave as described above the external magnetic field has to be weak because strong magnetic fields destroy superconductivity. The field strength required, called the critical field or H_c, to cause a phase transition back to the normal state varies for different superconductors. This transition can happen in two different ways and which way it happens for a specific superconductor determines whether it is a type I or II (6).

A type I superconductor is a perfect diamagnet for all fields below H_c and immediately loses all superconductivity at the critical field (6). Examples of type I superconductors are lead and aluminium (10).

Type II superconductors have two critical fields called the upper (H_{c2}) and lower critical field (H_{c1}). Below H_{c1} this type will be a perfect diamagnet just as type I. Between H_{c1} and H_{c2} some magnetic flux will penetrate the superconductor without losing all the superconductivity. Any field bigger than H_{c2} destroys the superconductivity completely (6). The explanation for the mixed state phase was given in 1954 by Alexei Abrikosov (11) when he described how the magnetic field can penetrate the superconductor in the form of vortices. These vortices are composed of the "vortex core" that is in the normal state and around the core is a circulating super current. Since the core is in the normal state, a small magnetic flux can pass through. It turns out the flux through each vortex is exactly $\Phi_0 = \frac{h}{2e}$ (6). LSCO, which is studied in this paper, along with all other known superconducting cuprates, are type II superconductors (2).

2.3 BCS-Theory

The first real microscopic theory of superconductivity was made by J. Bardeen, L. N. Cooper and J. R. Schrieffer in 1957 and has been named BCS-theory. The theory is based on three discoveries: First Bardeen found that the force between electrons in a solid can be attractive as a result of interaction with phonons in the lattice, as long as the energy difference between two electrons are less than the phonon energy (12). Secondly Cooper discovered that two electrons outside a fully occupied Fermi surface will pair up due to this attractive force in so called Cooper pairs. Lastly Schrieffer wrote down a quantum wave function for a coherent state of Cooper pairs (6).
The physical explanation is that the two electrons in a Cooper pair combined has spin equal to zero and therefore they behave like bosons instead of fermions and condense into the same quantum state. This condensation creates an energy gap equal to the binding energy of Cooper pairs. If the thermal fluctuations are small enough the electrons will not be able to cross this gap and are as a result bound as Cooper pairs (13). The size of the energy gap can be found by solving the BCS Hamilton and at $T = 0$ the energy gap is (6)

$$\Delta = \frac{3.52}{2} k_B T_c \tag{3}$$

It is the Cooper pairs that act as the charge carriers in a superconductor and the energy gap prevents the collision scattering that normally leads to resistivity (13).
BCS-theory predicts that the critical temperature cannot be bigger than approximately 30 K since phonon-electron interaction is not strong enough to form Cooper pairs above this temperature, but superconductors with critical temperatures above 30 K have been found (2).

2.4 Cuprate superconductors

In 1986 Georg Bednorz and Karl Alex Müller discovered that $La_{2-x}Ba_xCuO_4$ (LBCO) became superconducting at above 30 K which was higher than any other known superconductor at the time. This was surprising for two reasons. The first reason is that LBCO is a ceramic which at room temperature is a insulator and the parent compound La_2CuO_4 (LCO) is antiferromagnetic (2). The second reason was because of the high T_c (13). The discovery earned them a Nobel prize in 1987 (14).

After their discovery, many other copper-oxides, also known as cuprates, have been found to be superconducting including $La_{2-x}Sr_xCuO_4$ (LSCO), with a critical temperature of 38 K when $x = 0.15$, and $YBa_2Cu_3O_7$ (YBCO) that has a critical temperature of 92 K (2). It is exactly the high T_c of these materials that have led to them being called high temperature superconductors. For low temperature superconductors, 4 K, liquid helium is needed to cool them below T_c but a critical temperature of 92 K or higher can be reached by cooling in liquid nitrogen (77 K) which is much cheaper to make and easier to work with (15).
The existence of high temperature superconductors like the cuprate YBCO with critical temperatures above 90 K prove that BCS-theory, which limits the critical temperature to about 30 K, is not a complete theory of superconductivity. These high temperature superconductors also have many properties that are not found in low temperature superconductors like a pseudo gap regime and d-wave gaps (2). Despite the fact that cuprates have been extensively studied in recent years, the exact reason that they are superconducting is not yet well understood.

3 Crystallography

In this project we used crystallographic tools as a part of testing our samples to find out what crystal structure they had. This section contains a short overview of the theory behind crystal structures and X-ray diffraction.

3.1 Crystal structures and lattices

We will briefly cover the basic of crystal structures and their relation to scattering and in our case X-ray diffraction. This section is based on "The Oxford Solid State Basics" (16).
A lattice is a two- or more dimensional periodic structure. In many common crystals, the atoms are arranged in a three dimensional lattice. A lattice is an infinitely big, periodic pattern of lattice points. All the lattice points have exactly the same environment. A three dimensional lattice can be described by three lattice vectors $\mathbf{a}$, $\mathbf{b}$, $\mathbf{c}$, their respective lengths a, b, c are called the lattice constants.
The lattice vectors also define the unit cell, which represent the part of the crystal structure that is repeated in the lattice. The volume of the unit cell is given by

$$V_0 = \mathbf{a} \cdot \mathbf{b} \times \mathbf{c} \tag{4}$$

Having a lattice, we can also describe families of parallel and equally separated planes that contain all latices points. To describe these planes we make use of the reciprocal lattice. Reciprocal lattice vectors are defined as

$$\mathbf{a}^* = \frac{2\pi}{V_0}\mathbf{b} \times \mathbf{c}, \quad \mathbf{b}^* = \frac{2\pi}{V_0}\mathbf{c} \times \mathbf{a}, \quad \mathbf{c}^* = \frac{2\pi}{V_0}\mathbf{a} \times \mathbf{b} \tag{5}$$

The reciprocal lattice vectors are defined such that if the dot product is taken between a lattice vector and its corresponding recirprocal lattice vector the result is 2π (e.g. $\mathbf{a}^* \cdot \mathbf{a} = 2\pi$) but if the dot product is with a reciprocal lattice vector corresponding to another lattice vector the result is 0 (e.g $\mathbf{a}^* \cdot \mathbf{b} = 0$). A vector of the reciprocal lattice is written as

$$\mathbf{G}_{hkl} = h\mathbf{a}^* + k\mathbf{b}^* + l\mathbf{c}^* \tag{6}$$

Where h, k, l are integers. This vector is normal to all planes of the 'family' hkl, that is to say all planes with a specific orientation and separation defined by the h, k and l values. The distance between the lattice planes of a specific family can be found to be

$$d_{hkl} = \frac{2\pi}{|\mathbf{G}_{hkl}|} \tag{7}$$

This separation affects the way an incoming wave may diffract from the lattice planes, as will be discussed more clearly in Section 3.3 on the next page.

3.2 Crystal structure of La_2CuO_4 and $La_{1.85}Sr_{0.15}CuO_4$

There are various ways that these lattices can look. The structures are divided into 7 crystal systems defined by the symmetric properties they have. (e.g. cubic, where all lattice vectors are equally long and the angles between them are 90°). These 7 system combined with 14 Bravais lattices and 32 crystal classes gives a total of 230 space groups that a crystal structure can fall into. Here we describe the two that are relevant for LSCO:

The tetragonal system is like a 3D rectangle, so all the lattice vectors have 90° angles between them and two of them are equally long, $a = b \neq c$ (17). The LCO crystal (and by extension the resulting LSCO crystal) can be in the tetragonal space group of *I4/mmm* also known as K_2NiF_4 structure (18). An illustration of LCO in the *I4/mmm* structure is seen on figure 2a on the following page.

LCO can also be found in a orthorhombic system and specifically in the space group *Cmca* (19). This system has 90° angles between all lattice vectors, but none of the vectors have the same length, $a \neq b \neq c$ (17). This structure can be seen on figure 2b on the next page.

The LSCO superconducting crystal is achieved by doping (or in layman terms 'replacing' some of the lanthanum) with strontium in the LCO crystal. Lanthanum has an oxidation state of 3+ and strontium has an oxidation state of +2. This means that Strontium gives one electron fewer than Lanthanum. This effectively creates the abssence of an electron, also called a 'hole' which leads to the CuO_2 layers being effectively hole-doped (20). How much strontium is doped in determines at what temperature LSCO becomes superconducting (2), specifically the highest critical temperature for LSCO, $T_c = 38\,\mathrm{K}$, is achieved for a doping of $\approx 15\%$ (21). In this project we will also dope in other rare earth metals with the same oxidation level as lanthanum which should not change this imbalance.

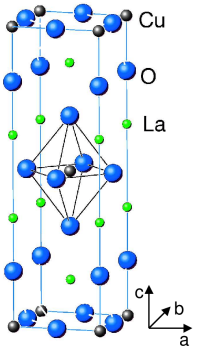

(a) Crystal structure of La_2CuO_4 in the *I4/mmm* structure (22).

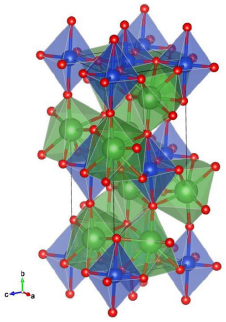

(b) Crystal structure of La_2CuO_4 in the *Cmca* structure (4). Blue is Cu, red is O and green is La

Figure 2: The two space groups that La_2CuO_4 can be found in relevant for this thesis. In this thesis, when other elements are doped in, and all goes well, then they replace the lanthanum.

3.3 X-ray diffraction

As described in Section 3.1 on page 4, crystals form lattices. The distance between parallel lattice planes is called d and it depends on the exact family of lattice planes (eq. 3.1). Now we will use these planes for understanding X-ray diffraction data. As two identical, incoming waves hit two adjacent planes from the same family. The waves have identical incident angles and reflection angles, θ, since both incident waves are identical and the planes are parallel see figure 3. One of the waves will hit the first plane and the other the will hit the second. The other wave will therefore travel an additional distance equal to $2d\sin\theta$. For the interference between the two waves to be constructive, then that extra distance has to be equal to an integer, n, times the wavelength of the waves, λ.

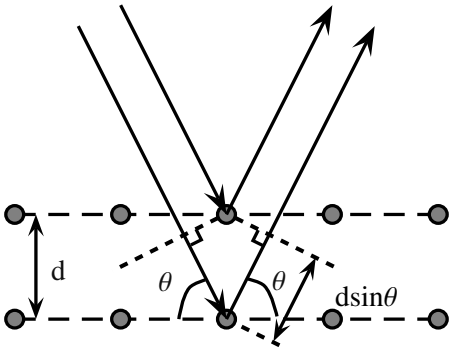

Figure 3: The geometrics of Bragg scattering, adapted from (16).

This gives what is known as Bragg's Law (16):

$$n\lambda = 2d\sin\theta \tag{8}$$

When the condition set by Bragg's law is met, then the reflected intensity at that angle will be much higher. Peaks stemming from this condition are called Bragg peaks. The intensity of the peak stems from how the X-rays interact with the atoms in the crystal. X-rays scatter from the electrons in the crystal. This intensity is proportional to the absolute square of the structure factor, $I_{hkl} \propto |S_{hkl}|^2$ (16) and this factor is related to the atomic number and position of each atom.

3.4 Powder X-ray Diffraction (PXRD)

In powder diffraction the X-ray diffraction pattern is 1-dimensional, this is due to the powder not being one single crystal. Rather it is a collection of numerous, randomly oriented, small crystallites. The planes that meet the condition of Bragg's law will result in a collection of scatterings from many different d-spacings called a Debye-Scherrer cone around the possible angle 2θ it could scatter. If you then cut the cone from the center defined by the incident wave and out, you obtain a 1-dimensional diffraction pattern with the intensity as a function of the deflected angle, 2θ.

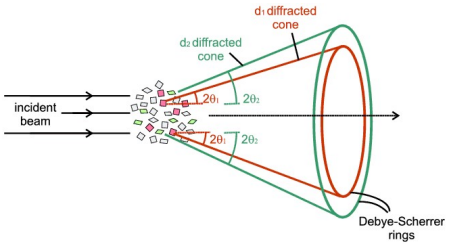

Figure 4: Bragg scattering of random crysallites forming a ring corresoping to each deflection angle $2\theta_i$. Figure from (23).

Due to the crystal symmetries, some of the lattice planes become equivalent and give peaks at the same deflected angles. This results in the intensity being proportional to the absolute square of the structure factor times the multiplicity of the given family of planes, M_{hkl} (16),

$$I_{hkl} \propto |S_{hkl}|^2 M_{hkl}. \tag{9}$$

3.4.1 Rietveld refinement

Given some powder X-ray diffraction data, plotting intensity versus 2θ, one can use Rietveld refinement to find the given crystal phase. To do this a theoretical model of a cyrstal structure with a certain space group is fitted to real data. This is done by changing the unit cell parameters (giving the peak positions), background, scaling factor, the integrated intensity and the peak shape of all Bragg peaks at a given point. This is what gives y_i^{calc}, while y_i^{obs} is the observed data.

The refinement is done by minimising a non-linear least squares function, where each data point has a weight usually stemming from the variance of data, $w_i = \frac{1}{\sigma^2(y_i^{obs})}$. The least square function that is minimised is given as

$$\Phi = \sum_i^N w_i \left(y_i^{obs} - y_i^{calc}\right)^2. \tag{10}$$

One way to estimate the quality of a Rietveld refinement is by the weighted profile R-factor (R_{wp}) (24)

$$R_{wp}^2 = \frac{\sum_i^N w_i \left(y_i^{calc} - y_i^{obs}\right)^2}{\sum_i^N w_i y_i^{obs}} \tag{11}$$

4 Material synthesis

To have materials to characterise and test we need to synthesise them. To synthesise those materials we need to give a short introduction into what high entropy materials are and what crystal structures you might find them in.

4.1 High entropy materials

Creating materials with high entropy is an emerging area in chemistry based on a simple principle. Changes in Gibbs free energy, which is given by $\Delta G = \Delta H - T\Delta S$, shows that at high temperatures a high entropy phase becomes thermodynamically favourable, as it dominates the minimisation of the free energy.

Making use of this thermodynamical principle, one can synthesise a product of these high entropy materials instead of having the end compound be a mixture of different enthalpically favoured compounds (25).

For our synthesis we utilise the Sol-Gel method. In it we have a mixture of our reactants in the form of nitrates dissolved in nitric acid and water. The end product then easily becomes homogeneous compared to other methods, where the reactants are in solid form that is mortared into a homogeneous form (precursor). The precursor is then both in our method and others heated to promote the high entropy phase. The Sol-Gel method makes it easier to obtain a homogeneous mixture before heating (26).

4.2 Ruddlesden-Popper Phases

This section is based on section 2.03 from "Comprehensive Inorganic Chemistry II" (27).
I4/mmm is a known Ruddlesden-Popper (RP) space group. In short a RP phase is one in which there is alternate stacking of two structures: a rock salt (RS) layer and perovskite (PE) layer.

The amount of perovskite subcells in the perovskite layer is signified by n, for $n = 1$ we have the K_2NiF_4 structure. As n increases, the size of the perovskite layer increases and with it, usually, the c value increases. This can be seen by some data tables from the text. Specifically LSCO has a value $c \approx 13$ Å and for a NdSrCuO-like structure where it has $n = 2$ perovskite subcells in

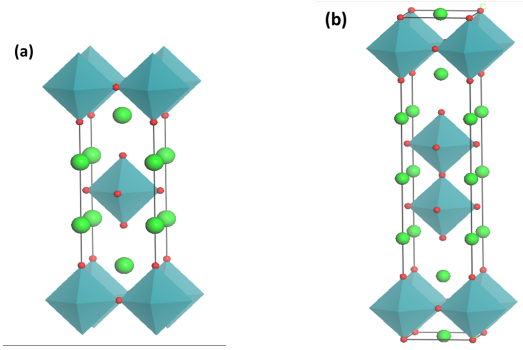

(a) Sr_2RuO_4 (n=1) **(b)** $Sr_3Ru_2O_7$ (n=2)

Figure 5: Ruddlesden-Popper Phases with n=1 and n=2 (28). Blue is Ru, red is O and green is Sr.

the perovskite layer and $c \approx 20\,\text{Å}$. One can regard figure 5 on the preceding page where the RS layers are the top and bottom blue 'diamonds' representing Ru, and the PE layer is the area in between with the green balls representing Sr sorrounding n 'diamonds'. In our project it is Cu instead of Ru and La doped with Sr instead of pure Sr.

4.3 Samples

Using the specific Sol-Gel method described in the following section we aimed to synthesise five mmol samples of four different materials:
$La_{1.85}Sr_{0.15}CuO_4$ (KAC-1),
$La_{0.925}Nd_{0.925}Sr_{0.15}CuO_4$ (KAC-2),
$La_{0.6166}Nd_{0.6166}Eu_{0.6166}Sr_{0.15}CuO_4$ (KAC-3) and
$La_{0.4624}Nd_{0.4624}Eu_{0.4624}Sm_{0.4624}Sr_{0.15}CuO_4$ (KAC-4).

To avoid writing out the long name, and because we are not certain that these are the actual materials that were produced in the synthesis, we will call them by the names KAC-1, -2, -3 and -4 when we reference them from now on.

Doing the synthesis process we made 6 different samples. The reason was that the first time we made $La_{0.925}Nd_{0.925}Sr_{0.15}CuO_4$ the wrong amount of neodymium was used. We also later chose to redo $La_{1.85}Sr_{0.15}CuO_4$ because we saw an anomaly in the data and wanted to see if it persisted with a new synthesis, which it did. In the rest of this thesis we will only analyse on the samples that were made correctly, which means we use the second synthesis of both KAC-1 and KAC-2.

4.4 Sol-Gel method

This section describes the method with which the samples of high entropy cuprates were synthesised.

The first step is to calculate the specific amount of nitrates, Nitric acid, demineralised water and sorbitol needed in the synthesis. The choice of nitrates depend on which rare earths were used for the samples, however copper nitrate, strontium nitrate and lanthanum nitrate is used in every sample. To calculate the weight needed for each compound we used the molecular weight of the compounds and the number of moles of cuprate. The method for calculating how much of each compound is needed can be found in Appendix 8.2 on page 30 as a Python code.

When the appropriate calculations were made the weighing of the chemicals began. The first thing to weigh was the water needed in a 100 ml glass beaker. The water and nitric acid should both evaporate away and their weights were not as important to measure accurately. Thus their measurements did not need to be as precise as the weighing of the other chemicals and was therefore done on a less precise scale. The nitrates and sorbitol were weighed at a precision of ± 0.0004 g. Lastly nitric acid was added using a pipette.

Because the actual weight used in the experiment might differ from the calculated values, a table (table 1 on the following page) was made to show both the calculated value and the weight used in the mixture. This table is only for $La_{0.4624}Nd_{0.4624}Eu_{0.4624}Sm_{0.4624}Sr_{0.15}CuO_4$, which is the high entropy compound, and the rest can be found in Appendix 8.1 on page 29. To make sure that all the compounds were transferred to the the beaker a few extra drops of water was used. This should not be a problem for the synthesis.

(a) Calculate needed amount of reactants

(b) Measure out and mix the needed reactants

(c) Put in glycerol bath at 90°C, until it forms blue foam

(d) Put in oven overnight at 250°C

(e) Mortar until the texture is creamy

(f) Put in oven for 20 hours at 1000°C

Figure 6: A simplified step by step guide of the Sol-Gel Method

When all the compounds had been weighed and added to the beaker a magnet was added as well and the beaker was put in a glycerol bath. By using a magnetic stirrer, with a built in heater, the glycerol bath was heated to 90°C in a fume hood. The mixture was heated in the bath for approximately 1.5 hours after which it turned into a blue foam (or gel) see figure 6c. The blue colour comes from the copper nitrate.

After this the beaker was placed in an oven set to 250°C overnight. The oven had an exhaust system since heating the sample produced toxic gasses. The next day the sample was taken out of the oven and transferred into a mortar where it was ground into a fine powder that had a creamy texture.

The last step was to put the powder into a alumina crucible and heat it at 1000°C for 20 hours to calcinate the sample. In our experiment the ramping speed for the oven was 50 $\frac{\mathrm{K}}{\mathrm{min}}$. Afterwards the powder was mortared again to make sure it was a fine powder and mixed as well as possible. The crystalline structure we aimed for should then have formed and this was checked by doing X-ray diffraction.

	Calculated	Measured
$La(NO_3)_3 \cdot 6H_2O$ [g]	0.3337	0.3337
$Sr(NO_3)_2$ [g]	0.0529	0.0533
$Nd(NO_3)_3 \cdot 6H_2O$ [g]	0.3378	0.3376
$Eu(NO_3)_3 \cdot xH_2O$ [g]	0.2605	0.2607
$Sm(NO_3)_3 \cdot 6H_2O$ [g]	0.3425	0.3429
$Cu(NO_3)_2 \cdot 3H_2O$ [g]	0.4027	0.4029
Sorbitol [g]	1.2050	1.2050
H_2O [ml]	25.8	25.82
Concentrated HNO_3 [ml]	3	3

Table 1: $La_{0.4624}Nd_{0.4624}Eu_{0.4624}Sm_{0.4624}Sr_{0.15}CuO_4$ (KAC-4)

4.5 PXRD-data and refinement

In this section we present the results and analysis of the PXRD from our samples. This should tell us something about what structures formed in the synthesis.

The X-ray diffractometer used to obtain the data was a Bruker D8 ADVANCE. The radiation source is CuKα_1 and CuKα_2 which gives wavelengths of 1.5405 Å and 1.5443 Å. The mea-

surements were taken from 10° to 70° over a four hour period. For the refinement we used the program GSAS-II, which is an open source Python based program (29). To do the refinement, a data file with a measurement of Al_2O_3 was used as a standard to determine the instrument specific parameters. These parameters were used when making all refinements. Then Crystallographic Information Files (CIFs), that describe the potential parent compounds, were gathered from the Inorganic Crystal Structure Database (ICSD). These information files could then be used to construct the theoretical diffraction patterns for those compounds using GSAS-II. These theoretical diffraction patterns were then analysed to see if they fit the observed diffraction data to see what phases might be present in the samples. The models could then be refined to better describe the actual crystal structures present in the samples.

The refined parameters in this Rietveld refinement were: Unit cell dimensions (a, b, c), phase fraction, microstrain, histogram scale factor, background and atomic displacement. The plots in figure 7 and 8 on the following page, were made directly in GSAS-II. All results of the PXRD-diffractions are summed up in table 2 on page 14 and the error given, is the estimate standard deviation calculated by GSAS-II.

The first sample KAC-1 was the control sample where we made $La_{1.85}Sr_{0.15}CuO_4$ to see firstly, if the method worked for making a well known superconductor and secondly, to use the result as a base CIF to refine the other samples from and lastly, a benchmark for the superconducting properties of the other samples. Since LSCO has been synthesised many times, CIFs of this specific doping were available as the starting model for the refinement. The diffraction data along with the refined model can be seen in figure 7 on the following page and the refined values for the structure can be seen in table 2 on page 14 under KAC-1.

In general this refinement was a success. The unit cell parameters was not changed much during the refinement, the R_{wp} value is 7.352 (table 2 on page 14) and it is also a good visual fit. All this shows that it is LSCO that has been synthesised. There is one small peak at $2\theta \approx 33°$, which is not accounted for in the theoretical model. Further discussion on this can be found in the discussion (Section 6.3.1 on page 22).

When it comes to the three other samples it was not as easy to find a starting structure to refine with and many different structure files were tried. The best fit, judged both on R_{wp} value and a visual fit, shows that all of them have created two phases or more instead of one. This fact has made it hard to make any definite conclusions about what the chemical structure is, but some general inferences can be made.

The first thing is that both KAC-2 and KAC-3 seem to have formed a orthorhombic phase (*Bmab*), which has a lower symmetry than the tetragonal *I4/mmm*. The *Bmab* is a non standard setting and is a result of the standard *Cmca* (space group 64) rotated 90°around the a-axis (17).

When looking at the phases with space group *I4/mmm* (table 2 on page 14) there are two different kinds. For KAC-2 and KAC-4 a phase has formed with a c-value in the unit cell of 19 to 20 Å where the other phases are around 13 Å. This could probably be because it formed a Ruddlesden-Popper phase with $n = 2$ instead of with $n = 1$ (27). This is supported by the paper by Grasmeder & Weller (31), from which the CIF fitted to KAC-2 stems, says that the structure type is isostructual with $La_2SrCu_2O_6$ which is a Ruddlesden-Popper phase with $n = 2$ (27).

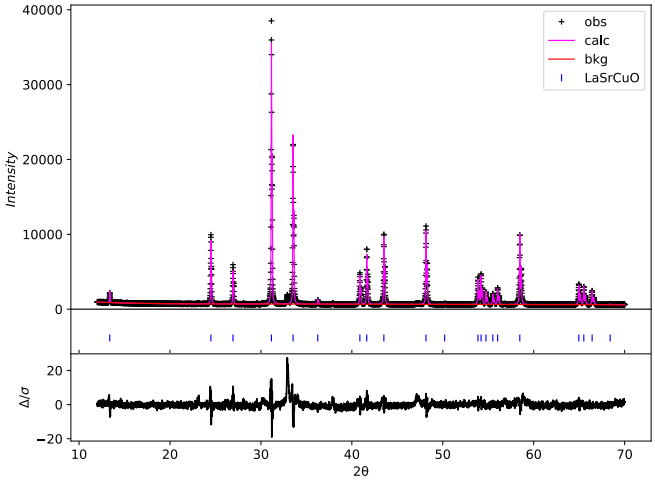

Figure 7: PXRD data for KAC-1. On the plot calc is the refined model, bkg is background, obs is the intensity data, LaSrCuO refers to where Bragg peaks should be for $La_{1.85}Sr_{0.15}CuO_4$ and the $\frac{\Delta}{\sigma}$ is the difference between observed and calculated weighted with the variance of the measurement.

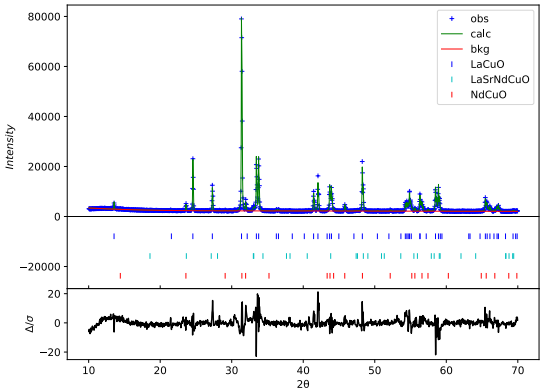

(a) KAC-2

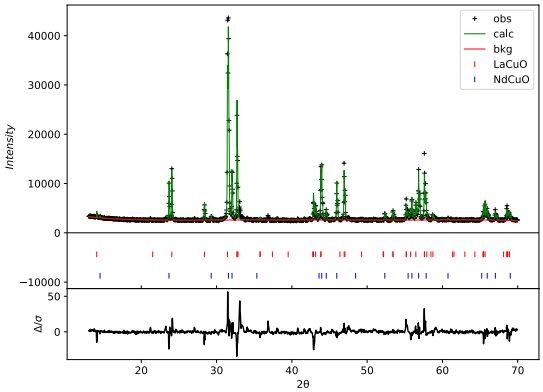

(b) KAC-3

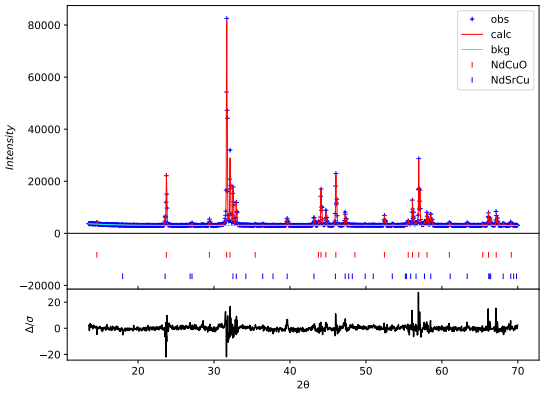

(c) KAC-4

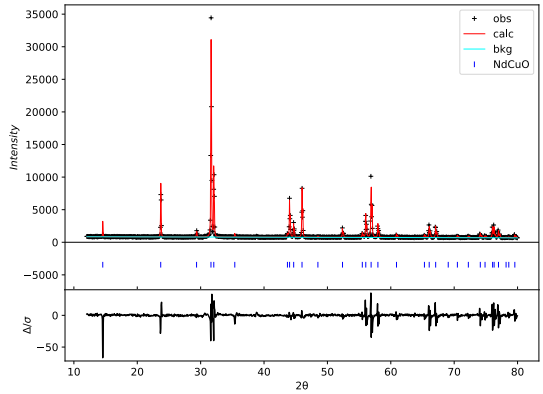

(d) HEO with M_2CuO_4 as parent (30)

Figure 8: PXRD-data and fit for the synthesised materials with the plot of a high entropy material for comparison. The legend is the same as with KAC-1 (figure 7).

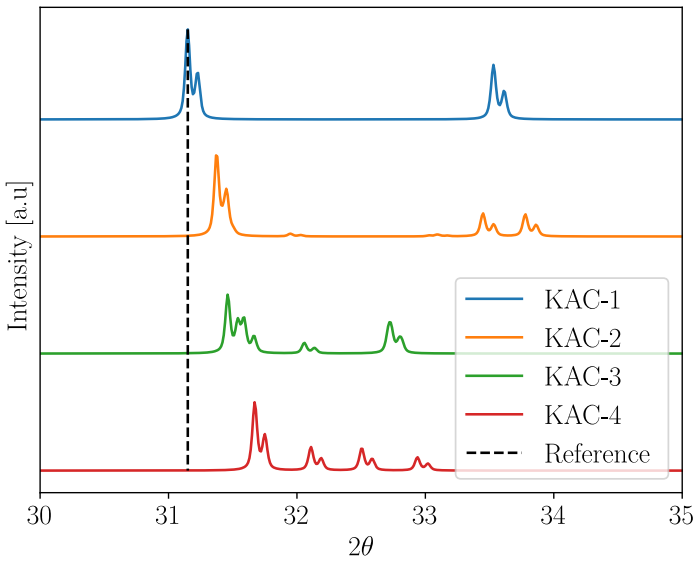

Figure 9: Zoomed in plot showing the refined placement of the main peaks of KAC-1, -2, -3, -4 compared to a reference $2\theta = 31.15°$

In the refinement we can see that the general trend in the c-value is that it gets smaller as more rare earth elements are doped in. This is expected since the dopants have smaller atomic radii than lanthanum (32). The exact values of the unit cell sizes can be seen on table 2 on the next page, but for a more visual representation the refined phases have been displayed on figure 9. This plot is zoomed in around the main peak for all four samples and shows how the peak move further right as more rare earth elements are introduced. This is in accordance to Bragg's law (eq. (8)), where a smaller distance, d, should give a bigger θ given that the rest of the values stay the same.

We see two trends in the difference between the unit cell sizes that we have before and after refinement. For the two lanthanum based phases, La_2CuO_4 and $LaSrNdCu_2O_6$, that we used as starting mdoels, the c-value is significantly smaller after refinement. For example the c-value for La_2CuO_4 is 13.2074 Å but in KAC-3 it is refined to be 12.5650 Å, which is a 5% difference. While for the neodymium based starting model, Nd_2CuO_4 and $Nd_{1.8}Sr_{1.2}Cu_2O_6$, it is a different story. In KAC-2 and -3 the unit cell size is bigger after refinement while for KAC-4 it is a little bit smaller but not by much and the $Nd_{1.8}Sr_{1.2}Cu_2O_6$ unit cell is still bigger.

These changes in unit cell sizes indicate that the composition of the phase in our materials is not the same as the starting model. It is therefore important to note that even though we have named the phases in table 2 on the next page and in this text after the parent phase, the refinement of the unit cells shows that there are probably other elements doped into the structure. It is very hard to find out what the structure is because of the impurities and not knowing which phase contains which elements. We have been unable to find any other literature where people have tried synthesising these materials and therefore have very little to compare it to. What we do know is that high entropy cuprates of this kind has been synthesised using the Sol-Gel method (4) and the results of such a synthesis (without strontium) can be seen on figure 7d on the preceding page and shows a single phase. These results are discussed in Section 6.3.1 on page 22.

Starting Model	Fraction	Space group	Starting cell [Å]	Refined cell [Å]	Volume [Å^3]	Strain
KAC-1, (R_{wp} = 7.352)						
$La_{1.85}Sr_{0.15}CuO_4$	1.00	*I4/mmm*	a = 3.7749(2) b = 3.7749(2) c = 13.2231(7)	a = 3.77665(2) b = 3.77665(2) c = 13.23543(8)	188.778(1)	0.002005
KAC-2, (R_{wp} = 5.324)						
La_2CuO_4	0.891	*Bmab*	a = 5.3512(3) b = 5.3881(3) c = 13.2074(8)	a = 5.35339(7) b = 5.30459(7) c = 13.0597(2)	370.860(6)	0.002607
Nd_2CuO_4	0.088	*I4/mmm*	a = 3.945(1) b = 3.945(1) c = 12.185(6)	a = 3.9583(2) b = 3.9583(2) c = 12.2709(9)	192.27(2)	0.002269
$LaSrNdCu_2O_6$	0.021	*I4/mmm*	a = 3.8540(1) b = 3.8540(1) c = 19.7688(6)	a = 3.832(2) b = 3.832(2) c = 19.09(2)	280.4(2)	0.007247
KAC-3, (R_{wp} = 7.645)						
La_2CuO_4	0.587	*Bmab*	a = 5.3512(3) b = 5.3881(3) c = 13.2074(8)	a = 5.4677(2) b = 5.4703(2) c = 12.5650(3)	375.82(1)	0.0021694
Nd_2CuO_4	0.413	*I4/mmm*	a = 3.945(1) b = 3.945(1) c = 12.185(6)	a = 3.9453(1) b = 3.9453(1) c = 12.1872(5)	189.696(9)	0.0024346
KAC-4, (R_{wp} = 3.879)						
Nd_2CuO_4	0.759	*I4/mmm*	a = 3.945(1) b = 3.945(1) c = 12.185(6)	a = 3.93896(3) b = 3.93896(3) c = 12.1429(1)	188.401(2)	0.0020432
$Nd_{1.8}Sr_{1.2}Cu_2O_6$	0.241	*I4/mmm*	a = 3.8404(6) b = 3.8404(6) c = 19.6190(30)	a = 3.84263(8) b = 3.84263(8) c = 19.7200(6)	291.18(1)	0.0022208

Table 2: Summary of the refined parameters for the four samples. The name under phase is not necessarily the material in the sample, but the name of parent structure used as a starting point for refinement.

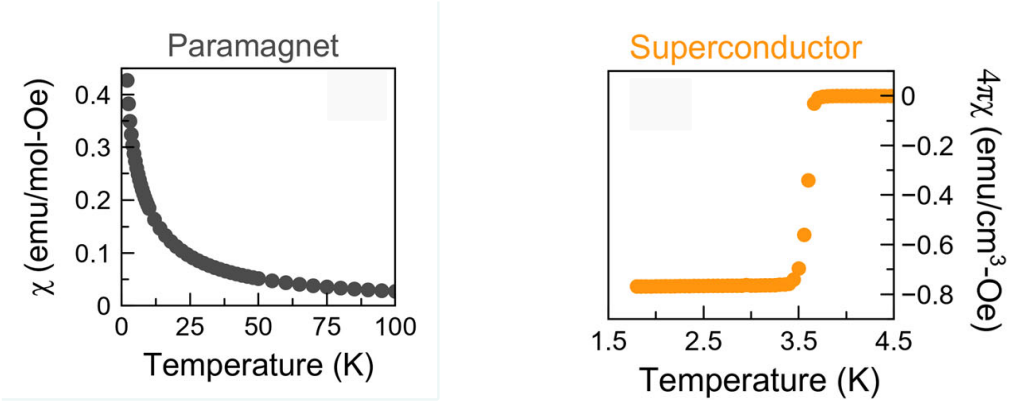

(a) $SrMn_{1/2}Te_{3/2}O_6$ **(b)** $PbTaSe_2$

Figure 10: Examples of two different susceptibility data sets with trends we might also see in our data (33).

5 Magnetic properties

The second part of testing is to measure the magnetic properties of the samples. We do this to find out if the samples are superconducting and if not what magnetic properties they might have.

5.1 Magnetism

This section is based on the information from the paper: "Tutorial: a beginner's guide to interpreting magnetic susceptibility data with the Curie-Weiss law" (33).

There are different ways to characterise the magnetic properties of materials. The focus in this project is magnetic susceptibility because of superconductors' relation to the Meissner-Ochsenfeld effect. We also assume, as is convention, that the materials magnetisation and the applied field is linearly proportional.

$$\mathbf{M} = \chi \mathbf{H} \tag{12}$$

There are a few different contributions that can influence the susceptibility of a material.

Orbital diamagnetism occurs in all materials and happens because the electrons have a tendency to repel magnetic fields. The effect is normally small and on the scale of -10^{-6} $\frac{\text{emu}}{\text{mol}}$ which means that it is normally overshadowed by other magnetic properties and can be ignored most of the time. A diamagnetic material is a material without any other contributions to the susceptibility.

If the material is superconducting we should see the susceptibility going from zero and then abruptly dropping to negative values as illustrated on figure 10b. This is because superconductivity makes a material a perfect diamagnetic with a susceptibility of -1 when measured in SI units but it is convention to measure using the electro magnetic unit (emu) which is a [cgs] unit. The susceptibility of a perfect diamagnet becomes $-\frac{1}{4\pi}$ when using [cgs].

Curie-Weiss paramagnetism is present only in magnetic materials which in this case refers to materials with unpaired electrons. The is characterised by the Curie-Weiss law

$$\chi = \frac{C}{T - \theta_{CW}} \Leftrightarrow \chi^{-1} = \frac{T}{C} - \frac{\theta_{CW}}{C} \tag{13}$$

Where C is the Curie constant and θ_{CW} is the temperature where the susceptibility diverges and is called the Curie-Weiss temperature. θ_{CW} can have both positive and negative values depending on the strength of the magnetic interactions between the ions in the material. Positive values means that the material has ferromagnetic interactions between ions and a negative value means the interactions are antiferromagnetic.

We will firstly look for the expected diamagnetism of a superconductor. If it instead shows paramagnetic traits, as in figure 10a on the previous page, then we will use the Curie-Weiss law because rare earth magnets normally follow that law. It should be noted that it might not be the only contribution.

Other contributions to magnetic behaviour could be: Van Vleck paramagnetism, Pauli paramagnetism and/or temperature-dependent itininerant moment paramagnetism. To take some difference from strict Curie-Weiss behaviour into account in the data analysis we will fit a modified Curie-Weiss law to the inverse susceptibility. The reason why we use the inverse susceptibility is that it should be linear as a function of temperature, as seen in equation (eq. (13)), if there is no other contribution. Divergence from a linear relation is easier to see than from an inverse proportional relation that Curie-Weiss susceptibility normally is. With the modified law we will be able to see if there is any temperature independent contribution to the susceptibility.

$$\chi = \frac{C}{T - \theta_{CW}} + \chi_0 \Leftrightarrow \chi^{-1} = \frac{T - \theta_{CW}}{\chi_0 \cdot (T - \theta_{CW}) + C} \tag{14}$$

The temperature independent term could come from many places, some of our samples have Eu^{+3} and Sm^{+3}, which can create strong temperature independent Van Vleck paramagnetism.

5.2 SQUID

To measure the susceptibility we used a SQUID (Superconducting QUantum Interference Device). This text is based on "Superconductivity, superfluids, and condensates" (6).

To explain how a SQUID works, we will first begin with describing the Josephson effect. The effect is a quantum tunnelling effect of electrons tunnelling between two superconductors, one to the left and one to the right, separated by an insulator. Electrons tunnel between the superconductors across the insulating layer with a probability proportional to $\sim e^{i(\theta_r - \theta_l)}$ for tunnelling from the right to the left and $\sim e^{i(\theta_l - \theta_r)}$ for the left to right, where θ describes the phase. Adding the two contributions together and remembering these are electrons, one gets a current that depends on the phase difference between the two superconductors. In Josephsons derivation he more specifically found a maximum called the critical current, I_C. Driving a current above the critical current will cause voltage to develop and the phase difference will change steadily.

$$I_{Josephson} = I_C \sin(\theta_r - \theta_l) \tag{15}$$

In a circuit one calls this setup, two superconductors separated by an insulator, a Josephson junction. A setup with two Josephson junctions in parallel is called a SQUID. The magnetic flux through the ring made by the two junctions is proportional to a difference between the phase differences in each junction, $\Phi = 2\pi\Phi_0(\Delta\theta_1 - \Delta\theta_2)$, where $\Phi_0 = \frac{h}{2e}$, is the flux quantum. Using

this and assuming the SQUID is balanced (both junctions have the same I_c) one can derive the critical current of the SQUID ring to be:

$$I_c(\Phi) = I_0\left|\cos\left(\frac{\pi\Phi}{\Phi_0}\right)\right| \tag{16}$$

Where I_0 is the driving current. If the current through a SQUID is higher than $I_c(\Phi)$, then there will be a voltage over the squid. This voltage depend on the current and therefore it also depend on the flux. When using the SQUID to measure the flux the sample is vibrated up and down in a coil. This gives a change in flux in the SQUID, which in turn gives a change in voltage.

5.3 Susceptibility data

To analyse the magnetic properties of our samples we made use of Bo Iversen's group's SQUID, more specifically the MPMS3 SQUID Magnetometer from Quantum Design.
We performed suseptibility measurements on all samples at 5 Oe using both Zero Field Cooled (ZFC) and Field Cooled (FC) samples. The KAC-2 measurements encountered a glitch such that the data seemed more exciting than they were and therefore we originally investigated KAC-2 closer and have a lot of data on it. KAC-2 and -3 both got measurements at 10 Oe as well. KAC-2 and -4 both had M vs H measurements done at various temperatures.

To make measurements with the SQUID, the sample was prepared by putting a bit of it into a vial and weighing it on an accurate scale. Then the vial was put in a holder and centered. Then it was put on a long rod that was inserted into the MPMS3. The MPMS3 was then programmed to run a series of experiments in succession before the sample was switched out.

ZFC measurements were done by oscillating a strong field between positive and negative before letting it slowly diminish in strength to a value as close to zero as possible. This was done to have little to no remnant field left. The sample was then cooled to the lowest temperature possible for MPMS3 (1.8 K) (34), the chosen field strength (e.g. 5 Oe) was applied and the resulting moment was measured by the SQUID as the temperature was slowly raised to a 'high temperature' of 40 K for most measurements, since optimally doped LSCO has a critical temperature of 38 K (6). We did not anticipate finding superconductivity at higher temperatures for our samples Then the sample was cooled under the applied field and then heated again to make the FC measurement.

The data from the SQUID was then analysed and visualised into plots using Python. We find the molar susceptibility of our samples from the magnetization and applied field via the formula:

$$\chi_{mol}\left[\frac{\text{emu}}{\text{mol}_\text{N}\text{Oe}}\right] = \frac{M[\text{emu}]}{H[\text{Oe}]}\left(\frac{M\left[\frac{\text{mg}}{\text{mol}}\right]}{m[\text{mg}]\cdot n}\right) \tag{17}$$

Where the first M corresponds to magnetization and the second to molarmass. n is the number of magnetic ions, we use $n = 1$ as we don't know the number. For this reason we measure susceptibility per formula unit (f.u.) (33).

5.3.1 The phase transition of KAC-1

KAC-1 showed a superconducting phase transition that starts sharp but then slows down. If the crystal was homogeneously doped, then we would expect a very sharp transition like figure 10b

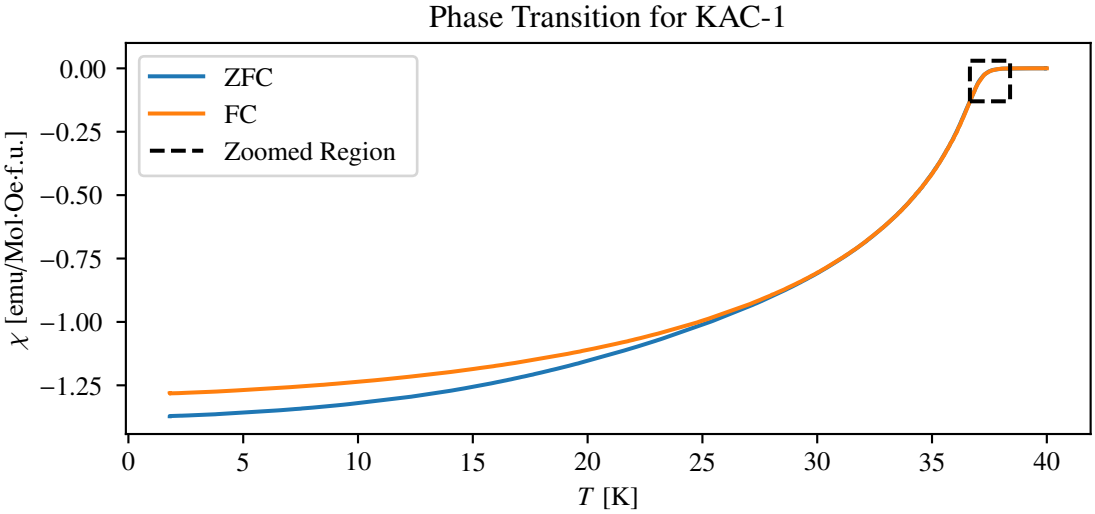

(a) Zero- (blue) and Field Cooled (orange) susceptibility measurements of KAC-1

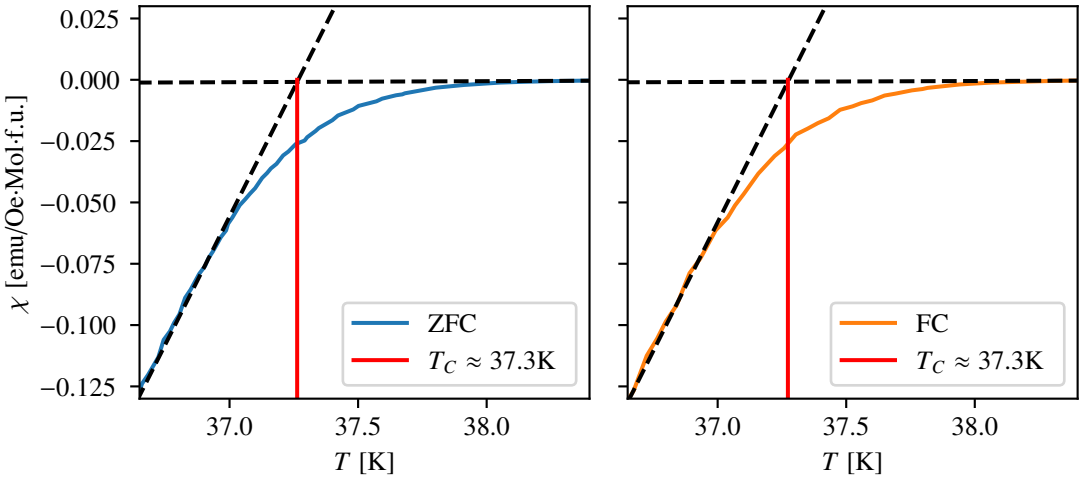

(b) Onset critical temperature of Zero- (left) and Field Cooled (right)

Figure 11: Susceptibility data for KAC-1, showing a phase transition

on page 15. The ZFC and FC susceptibility approach a value of $\chi \approx -1.3 \frac{\text{emu}}{\text{molOe}}$ and $\chi \approx -1.2 \frac{\text{emu}}{\text{molOe}}$ respectively.

The onset critical temperature of KAC-1 was found by making two linear fits, one for the plateau and one for the beginning of the descent in susceptibility. This critical temperature is $T_c \approx 37.3\,\text{K}$ the uncertainty on that value is tiny $\sim 10^{-6}$ and was found using the variance formula and uncertainties stemming from covariance. The temperature was found to be approximately the same for both ZFC and FC, this can be seen on figure 13 on the next page.

5.3.2 The properties of KAC-2,-3 & -4

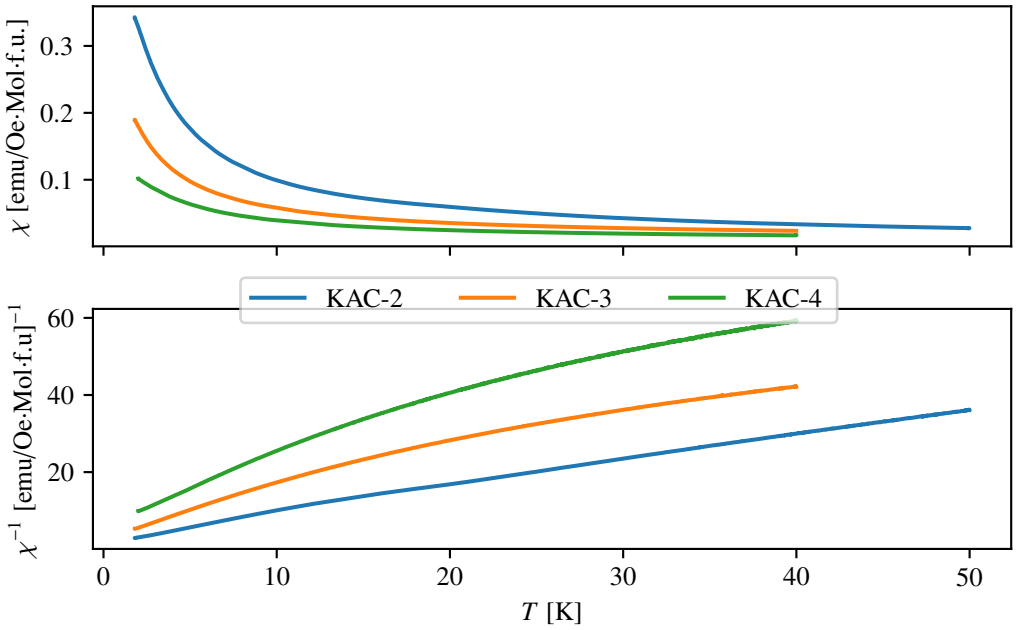

Figure 12: Plot of molar susceptibility per formula unit data, χ, and its inverse, χ^{-1}, for KAC-2, -3 and -4 at 5 Oe

Sample	θ_{CW}[K]	$C\left[\frac{\text{emu}}{\text{MolOe}}\text{K}\right]$	$\chi_0\left[\frac{\text{emu}}{\text{MolOe}}\right]$
KAC-2	−1.3189(1)K	1.05298(4)	0.008335(2)
KAC-3	−1.1293(2)K	0.52909(3)	0.010515(1)
KAC-4	−2.0787(6)K	0.39256(5)	0.007136(2)

Table 3: Table of values from Curie-Weiss fit to χ^{-1}. Uncertainties stem from propagated uncertainties using the variance formula

Neither KAC-2, -3 or -4 showed any superconducting phase transition within the range of measurement (figure 12). They only displayed paramagnetic behaviour that we could describe by the Curie-Weiss law (eq. (14)). It is apparent from the inverse susceptibility in figure 12 that they are not linear, specifically they seem to slow down as temperature increases, this corresponds

to the temperature independent contribution, χ_0, being positive. The characteristic, θ_{CW} for the samples were fitted and can be found in table 3 on the preceding page.

5.3.3 M vs H for KAC-2 & -4

The magnetisation response to an applied field of KAC-2 and -4 at various temperatures and plotted in figure 13. The magnetization vanished with the applied field as its strength became zero. This shows that neither of the samples are ferromagnetic in nature, KAC-4 is however not linear at low temperature and strong applied field.

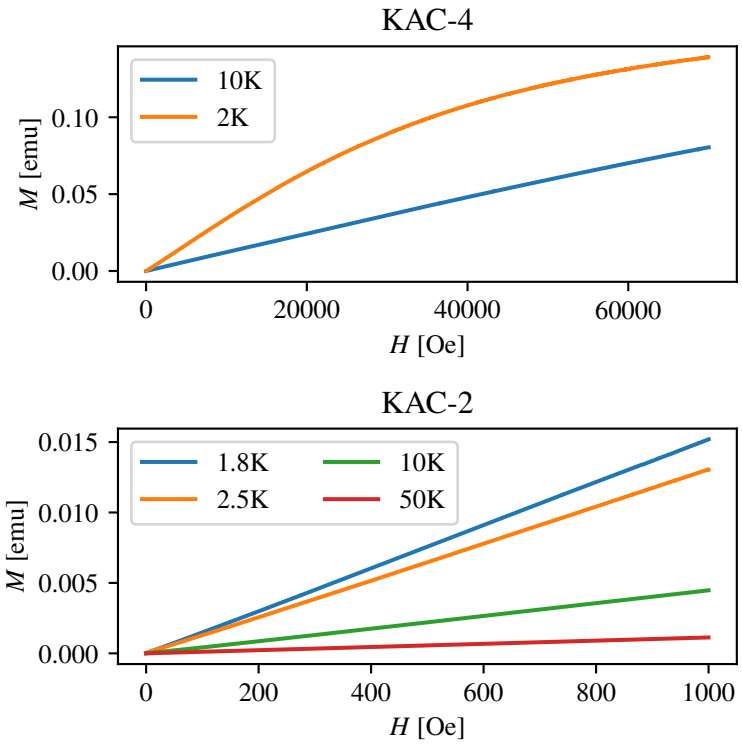

Figure 13: M vs H data at various temperatures for KAC-2 and -4

6 Discussion

There are many smaller aspects of this project so the discussion will be split up into subsections for the different parts.

6.1 Synthesis

The synthesis was only somewhat successful. The results show that we were successful in synthesising LSCO, but they also show that we did not succeed in making the high entropy materials we aimed for. One reason for this could be that the materials we tried to synthesise

have never been synthesised before so they might not be possible to synthesise. Some different choices in the synthesis could potentially change the outcome.

The calcination temperature we have used, 1000°C, could have been decreased or increased. The effect of that is that the domain size might respectively decrease or increase (30). The structures might be affected if heated too much, and the desired product therefore lost. In the report "Solid solution formation in the (La, Pr, Nd, Sm, Er)$_2$CuO$_4$ phase system", where the Sol-Gel synthesis method is from, a calcination temperature of 900°C was used, but it also showed results from a calcination at 700°C, but the samples were less crystalline than for the 900°C (4).

The choice of LSCO being doped with the rare earths Nd, Eu and Sm was based on them being similarly sized to La in their ionic radii while also having the same oxidation state (32) and because they have effectively been used in high entropy before (4). Nd was also chosen because it has been observed as a dopant in a superconducting LSCO sample before.

The Sol-Gel Method is not the only way to produce high entropic cuprates. Mazza, A., et al. used pulsed laser deposition to create high entropic cuprates of the A_2CuO_4 Ruddlesden-Popper type. This is the same type we have been studying but in film form. The dopants for the high entropic oxides are Pr, Nd, Sm, Eu, and then either Ce^{+4} or Sr^{+2} at concentrations known to induce superconductivity in their respective parent compounds Nd_2CuO_4 and La_2CuO_4. These high entropy oxides did not show superconductivity (35).

For the next part we will discuss the results for the different samples.

6.2 KAC-1

The synthesis of $La_{1.85}Sr_{0.15}CuO_4$ in KAC-1 was a success. The PXRD-data shows a good fit, that it is a single phase and the susceptibility data shows that it is indeed superconducting. The following are the points of discussion we would like to raise based on those results.

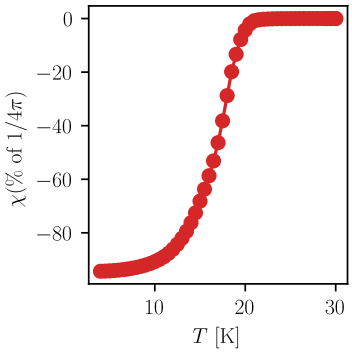

Figure 14: The bulk magnetic susceptibility measured at 20 G on a piece of underdoped (7%) LSCO, data from (36)

The transition for KAC-1 is not as sharp as what would be expected assuming it to be homogeneously doped. If we compare our data to another LSCO susceptibility curve at the transition like that found in figure 14, we see the difference in the sharpness of the transition. If instead we don't have homogeneous doping, then some parts of the crystal will begin to be superconducting before others, this will make the overall transition gradual just like the strontium doping is gradual throughout the sample.

The FC and ZFC measurement approaches a weird value of between -1.2 and -1.3, when it should be $-\frac{1}{4\pi}$. We suspect it could stem from confusion on the exact nature of the emu unit in this specific instance, an error in our calculation, or it could stem from the SQUID's calibration. We have not had the time to properly investigate the reason behind this peculiar value that the measurements approaches.

When it comes to the PXRD-results there is only a few things to mention. The R_{wp} is below 10 which is considered a good fit. There is some microstrain in the sample, which broaden the

peaks, but in general it was a very successful synthesis. One small point is the existence of the small peak at $2\theta = 33°$ (figure 7 on page 12). This peak was what made us redo the synthesis, but it was present at the same position both times we made the material. To try to account for the peak we did Rietveld refinement using CuO, LaO, SrO and other structures that might have formed, as starting models to see if the peak could be a small impurity, but none of them fitted the position of the peak. The persistence of the peak through different synthesises also makes impurities somewhat less plausible, but not impossible, since the same impurity would have to be made two times. The data for the original synthesis and second synthesis is both shown in Appendix 8.3 on page 31 zoomed in so the peak is visible.

We have been unable to explain why this peak is there, but in trying to find an explanation we found another bachelor thesis (37) that had found this peak as well when making this specific doping of LSCO. In that thesis the LSCO was made with another synthesis method. If we look at the other samples they also have peaks at around 33°, but for them they are explained by the phase fitted, which does not fit on KAC-1. A plausible explanation could be that it is the main peak of a different phase of LSCO that we have been unable to find. This could be a very small impurity since the peak is only 2000 in intensity at its highest and the main peak of the LSCO is almost 40000 so about 5% the intensity (figure 7 on page 12). This should not have a big impact on the superconductivity.

6.3 KAC-2, -3 & -4

We have chosen to discuss the rest of the samples together because they show many of the same behaviours in regard to the susceptibility measurements and some trends in the PXRD-data that only makes sense when viewing all three together.

6.3.1 Diffraction

The first thing to note is that we were not successful in synthesising these materials. The PXRD-data shows that we did not succeed in making any of the samples single phased. The R_{wp} values are all below 10 and for KAC-4 it is 3.879. This tells us that the refinement is very likely to be correct. This is also confirmed visually by the fact the few to no peaks are unaccounted for in the refinement.

We did observe some changes in the unit cell sizes. Some parameters got bigger and some got smaller in comparison with the starting model (table 2 on page 14). Some changes in the unit cell sizes were expected and we have addressed some of this in the analysis. We expect to see a reduction in unit cell sizes and that the reduction is greatest in the c-direction. This is since lanthanum sits between the CuO_2 layers along the c-direction in the crystal structure (figure 2 on page 6). Microstrain is also seen in all the samples. Microstrain is normally nonuniform strain which should not change the size of the unit cell.

When it comes to the fact that the synthesised compounds are not in general smaller than the neodymium based starting structure it could be because neodymium, europium and samarium have a smaller ionic radii than lanthanum and strontium (32) so as these elements are doped in the average unit cell sizes might look more like neodymium based compounds. The combination of all the elements might very well average out to the size neodymium alone would make.

The sizes of the ionic radii might also be a reason for the multiple phases we see. The large ions La and Sr are known to show a preference to occupying 4e sites in the rock salt layers. This is opposed to the smaller ion, Nd, which prefers occupying the 2a sites between the CuO_2 layers (38). This could be the reason why Nd orders in a different structure with larger c and why KAC-2 and KAC-3 have phases with lower symmetry. It might also be the reason for the creation of the Ruddlesden-Popper phase with $n = 2$ in KAC-2 and KAC-4. One way to combat this could be to choose other elements than Nd, Eu and Sm that have ionic radii closer to lanthanum. Further experiments are needed to find out if this could be a way to promote single phase samples.

In this regard it is also important to note that KAC-4, which technically would be the only real high entropy material since that definition requires 5 metals, only has phases in the space group *I4/mmm*. It forms two phases which is not ideal. The lower symmetry phases might not be problematic, if the aim is to make the high entropy materials as it was with this project. The reason we do not see any superconductivity in this sample could be because the strontium is not homogeneously mixed between the two phases. If that is the case then one phase might be over doped and the other under doped to the point where we would not see superconductivity in either.

We did consider trying to use the phase fractions and unit cell sizes to find out which elements where in each phase, but due to the number of variables we deemed that it was too hard to get a good result. The main problem would be that multiple elements together can average out to look like another single element. For example if we look at ionic radii of La ($r = 1.216$), Eu ($r = 1.120$) and Nd then $0.45 \cdot 1.216\text{Å} + 0.55 \cdot 1.120\text{Å} = 1.1632$ and neodymium's radii is 1.163. The ionic radii in this example is from (32).

In this next part we will discuss the susceptibility measurements for KAC-2, -3 and -4.

6.3.2 Susceptibility measurements

Even though KAC-2, -3 and -4 did not show any signs of being superconducting they still exhibited interesting magnetic properties that warrant discussion.

KAC-2, -3 and -4 all exhibited paramagnetic behaviour in accordance with Curie-Weiss paramagnetism. This is not unexpected but the specific values we have found are interesting. The parent compound LCO is antiferromagnetic so the doping of Sr, Nd, Eu and Sm must have had an effect on the magnetic properties (i.e making regular LSCO by doping LCO with Sr and making it superconducting instead.)

KAC-2, -3 and -4 had Curie-Weiss temperatures of $\theta_{CW} \approx -2\,\text{K}$. LCO by itself shouldn't have that strong a moment at low temperatures, as it orders to antiferromagnetic below 240K (Néel temperature) (39). This isn't entirely unexpected, as our samples also have significantly more rare earths present compared to regular LCO and rare earths don't really interact but have strong moments (33), which would have that effect. But the fact that they have negative Curie-Weiss temperatures tells us that they are not just paramagnets but they have antiferromagnetic tendencies. If we wanted to test the antiferromagnetic properties of the samples we would probably have to go to higher temperatures, but this was not part of the project.

The M vs H curves are linear and are therefore also consistent with paramagnetic behaviour.

KAC-4 is measured at so low temperaturs and such a high field that we can even see it starting to plateau this is expected as the paramagnetism can saturate under those conditions.

Another point is to look the Curie-Weiss constant, C. The Curie-Weiss constant is linked to the number of unpaired electrons and can tell us about the magnetic moment of the ions in the samples (33). The relation between C and the effective magnetic moment.

$$\mu_{eff} = \sqrt{8C}\mu_B[\text{cgs}] \tag{18}$$

The effective moment for LCO, which the structure of our samples KAC-2 and KAC-3 seem like, is $0.13\mu_B$ (40) and from our Curie-Weiss constants C in table 3 on page 19 we get $2.9023(1)\mu_B$ and $2.05737(7)\mu_B$ for KAC-2 and -3 respectively. This is significantly higher than for LCO alone. The initial explanation is that those samples aren't LCO, they only look like it but they have more rare earths. These rare earths might be the instigators of this effect.

Others have also been able to find paramagnetic behaviour at low temperatures, past the Néel temperature. They, however, were working with a single LCO crystal and had a significantly smaller change in susceptibility (on a scale of $\sim 10^{-4}$ compared to our $\sim 10^{-1}$). They found a Curie-Weiss temperature of $-1.2(2)$K which is on the same order of magnitude as our values (41).

The last point is that in the inverse susceptibility plots we see a very small temperature independent deviation from Curie-Weiss law. The χ_0 values (table 3 on page 19) are positive and of the order $\sim 10^{-2}$. This indicates that there is some small temperature independent paramagnetism in the samples. The two types of temperature independent paramagnetism mention in Section 5.1 on page 15 are Pauli and van Vleck paramagnetism which are normally on the scale of $\sim 10^{-4}$ to $\sim 10^{-5}$ (33). These effects are too small to be the only contributions to the temperature independent term. We have had some problem finding the out exactly what the emu unit is in our measurement, so it is not completely certain that these paramagnetic contributions would not be enough.

7 Conclusion

Using the Sol-Gel method, the synthesis of KAC-1 created a LSCO superconductor that had an onset critical temperature of $T_c \approx 37.3\,\text{K}$. This is close to the expected temperature of 38 K. The gradient in the susceptibility was not as sharp as could be expected and there is probably a gradient in the level of strontium doping in the sample.

The same method didn't create pure phases of the wished products KAC-2, -3 and -4, additionally, none of them showed any superconductive behaviour. Instead KAC-2 and KAC-3 formed partial LCO-like structures with some NdCuO-like structures and showed paramagnetic behaviour with some antiferromagnetic tendencies at temperatures below 50 K. KAC-4 showed the same magnetic behaviour but formed no low symmetry phases and instead formed two phases both in the $I4/mmm$ space group.

The fact that the created phases were not pure might be because of the preferences of site-occupancy from La, Sr and Nd that stem from the size of their ionic radii.

The general conclusion is that we were successful in synthesising the superconductor $La_{1.85}Sr_{0.15}CuO_4$ using the Sol-Gel method, but that we were unable to make any high entropy

cuprates and can therefore not make any conclusions about whether or not such a material would be superconducting.

7.1 Outlook

Our results leave a lot of open ended questions that could be explored further.

When it comes to measurements on the existing samples that could be considered was to do resistivity measurements as well as the susceptibility. The addition of resistivity measurements could give more insight. One thing it could be used for is to make absolutely sure that the samples do not become superconducting. The reason resistivity might show superconductivity when susceptibility does not is because superconductors have critical fields above which superconductivity is destroyed. It is highly unlikely though that resistivity would show anything else because we measured ZFC susceptibility on our samples at just 1.5 Oe. This would minimise the possibility of being above our samples' critical fields, and we still did not see superconductivity in any other samples than KAC-1. The original plan was to measure resistivity on the samples, but we did not have time to set up the cryostat we would have used to do it.

When it comes to what the next steps in making high entropy superconductors, one thing that could be tried in the future is to create these high entropy samples with different dopants to perhaps get a pure phase that might have superconductive properties. Another avenue up for exploring could be to oxygen dope high entropy oxides. This doping is known to create superconductors and is done after synthesis and could therefore be viable to use on already made high entropy oxides. A whole other direction could also be to try with different kinds of oxides. Recent theoretical research show the palladium oxides might be superconducting (42), so it might be interesting to make high entropy palladium oxides and test for superconductivity.

References

1. Bednorz, J. G. & Müller, K. A. "*Possible high T_c superconductivity in the Ba-La-Cu-O system*". **Zeitschrift fur Physik B Condensed Matter 64,** 189–193. doi:10.1007/BF01303701 (June 1986).
2. Keimer, B., Kivelson, S. A., Norman, M. R., Uchida, S. & Zaanen, J. "*From quantum matter to high-temperature superconductivity in copper oxides*". en. **Nature 518,** 179–186. doi:10.1038/nature14165. (01/30/2023) (Feb. 2015).
3. Zhang, Y. "*High-Entropy Materials: A Brief Introduction*", 1–8. ISBN: 978-981-13-8525-4. doi:10.1007/978-981-13-8526-1 (Springer, Jan. 2019).
4. Gjelsten, X. B., Kirsch, A. & Jensen, K. M. Ø. "*Solid solution formation in the (La, Pr, Nd, Sm, Er)2CuO4 phase system*". en. Student Project (University of Copenhagen, 2022), 1–7.
5. Mizuguchi, Y. & Yamashita, A. en. in Superconductivity in HEA-Type Compounds (ed Kitagawa, J.) (IntechOpen, Sept. 2021). ISBN: 978-1-83881-078-8. doi:10.5772/intechopen.96156. (06/12/2023).
6. Annett, J. F. "*Superconductivity, superfluids, and condensates*". ISBN: 978-0-19-850756-7 (Oxford University Press, Oxford ; New York, 2004).
7. Van Delft, D. & Kes, P. "*The discovery of superconductivity*". **Physics Today 63,** 38–43. doi:10.1063/1.3490499. (Sept. 2010).
8. Lefmann, K., Andersen, N. H. & Hedegaard, P. "*Hvorfor findes der høj-temperatur superledning?*" da. **KVANT 2007,** 15–17.
9. Meissner, W. & Ochsenfeld, R. "*Ein neuer Effekt bei Eintritt der Supraleitfähigkeit*". **Naturwissenschaften 21,** 787–788. doi:10.1007/BF01504252. (Nov. 1933).
10. Hauser, J. J. "*Measurement of the coherence distance of a pure type-I superconductor*". **Phys. Rev. B 10,** 2792–2798. doi:10.1103/PhysRevB.10.2792. (7 Oct. 1974).
11. A. Abrikosov, A. "*TYPE II SUPERCONDUCTORS AND THE VORTEX LATTICE*". in Nobel Lectures (Dec. 2003). URL: https://www.nobelprize.org/prizes/physics/2003/abrikosov/lecture/.
12. Bardeen, J., Cooper, L. N. & Schrieffer, J. R. "*Theory of Superconductivity*". en. **Physical Review 108,** 1175–1204. doi:10.1103/PhysRev.108.1175. (01/30/2023) (Dec. 1957).
13. Rohlf, J. W. "*Modern physics from α to Z^0*" 1st ed. ISBN: 978-0-471-57270-1 (John Wiley, New York, 1994).
14. "*The Nobel Prize in Physics 1987*". en-US. URL: https://www.nobelprize.org/prizes/physics/1987/summary/ (05/23/2023).
15. P.J. Ford, G. S. "*The rise of the superconductors*" 1st ed. ISBN: 0-7484-0772-3 (CRC Press, 2004).
16. Simon, S. H. "*The Oxford Solid State Basics*". en. ISBN: 978-0-19-968077-1 (Oxford University Press, London, England, June 2013).

17. Ravel, B. "*Understanding and denoting space groups — Artemis 0.9.26 documentation*". 2016. URL: https://bruceravel.github.io/demeter/documents/Artemis/atoms/space.html (06/04/2023).

18. Grande, B., Müller-Buschbaum, H. & Schweizer, M. "*Über Oxocuprate. XV Zur Kristallstruktur von Seltenerdmetalloxocupraten: La2CuO4, Gd2CuO4*". **Zeitschrift für anorganische und allgemeine Chemie 428,** 120–124. doi:10.1002/zaac.19774280116. (05/23/2023) (Jan. 1977).

19. Izumi, F., Kim, Y.-I., Takayama-Muromachi, E. & Kamiyama, T. "*Neutron powder diffraction study of phase separation in La2CuO4+δ*". **Physica C: Superconductivity 235-240,** 841–842. doi:https://doi.org/10.1016/0921-4534(94)91645-4. (1994).

20. Rømer, A. T. "*Magnetic correlations in the high-temperature superconductor La1.88Sr0.12CuO4*". M.Sc. thesis (University of Copenhagen, Aug. 2009).

21. Mohottala, H. E., Wells, B. O., Budnick, J. I., Hines, W. A., Niedermayer, C., Udby, L., Bernhard, C., Moodenbaugh, A. R. & Chou, F.-C. "*Phase separation in superoxygenated La2-xSrxCuO4+y*". en. **Nature Materials 5,** 377–382. doi:10.1038/nmat1633. (06/13/2023) (May 2006).

22. Grafe, H.-J. "*Nuclear Magnetic Resonance Studies of Rare Earth co-doped Lanthanum Cuprates*". M.Sc. thesis (Technischen Universität Dresden, June 2023), 31.

23. Barnes, P., Simon, J. & Vicker, M. "*Powder Diffraction*". 2016. URL: http://pd.chem.ucl.ac.uk/pdnn/diff2/kinemat2.htm (06/02/2023).

24. Dinnebier, R. E., Leineweber, A. & Evans, J. S. O. "*Rietveld refinement: practical powder diffraction pattern analysis using TOPAS*". OCLC: on1085670023. Chap. 2.1. ISBN: 978-3-11-045621-9 (De Gruyter, Berlin ; Boston, 2019).

25. Dragoe, N. & Bérardan, D. "*Order emerging from disorder*". **Science 366,** 573–574. doi:10.1126/science.aaz1598. (02/03/2023) (Nov. 2019).

26. Mackenzie, J. D. & Bescher, E. P. "*Chemical Routes in the Synthesis of Nanomaterials Using the Sol–Gel Process*". en. **Accounts of Chemical Research 40,** 810–818. doi:10.1021/ar7000149. (05/23/2023) (Sept. 2007).

27. Raveau, B. en. in Comprehensive Inorganic Chemistry II 63–102 (Elsevier, 2013). ISBN: 978-0-08-096529-1. doi:10.1016/B978-0-08-097774-4.00203-5. (05/23/2023).

28. Jasongoh. "*Ruddlesden-popper phase 1.png*". en. Page Version ID: 887218624. Mar. 2019. URL: https://en.wikipedia.org/w/index.php?title=File:Ruddlesden-popper_phase_1.png&oldid=887218624#metadata (06/13/2023).

29. Toby, B. H. & Von Dreele, R. B. "*GSAS-II : the genesis of a modern open-source all purpose crystallography software package*". **Journal of Applied Crystallography 46,** 544–549. doi:10.1107/S0021889813003531. (06/01/2023) (Apr. 2013).

30. Tegtmeier, M., Kirsch, A. & Jensen, K. M. Ø. "*Synthesis and Characterisation of New Rare Earth Element High Entropy Cuprates*". en. B.Sc Thesis (University of Copenhagen, 2022).

31. Grasmeder, J. R. & Weller, M. T. "*Structure and oxygen stoichiometry in Ln2-xSr1+xCu2O6-y (Ln = La, Nd, Sm) phases*". **Journal of Solid State Chemistry 85,** 88–99. doi:https://doi.org/10.1016/S0022-4596(05)80064-7. (1990).

32. Shannon, R. "*Revised Effective Ionic Radii and Systematic Study of Inter Atomic Distances in Halides and Chalcogenides*". **Acta Crystallographica Section A 32.** ISBN: 0108-7673, 751–767. doi:10.1107/s0567739476001551 (Sept. 1976).

33. Mugiraneza, S. & Hallas, A. M. "*Tutorial: a beginner's guide to interpreting magnetic susceptibility data with the Curie-Weiss law*". en. **Communications Physics 5,** 1–12. doi:10.1038/s42005-022-00853-y. (01/30/2023) (Apr. 2022).

34. Kunzmann, M., Appel, D. & Adler, T. "*MPMS3 SQUID magnetometer Quantum Design | Quantum Design*". EN. URL: https://qd-europe.com/de/en/product/mpms3-squid-magnetometer/ (06/15/2023).

35. Mazza, A. R., Gao, X., Rossi, D. J., Musico, B. L., Valentine, T. W., Kennedy, Z., Zhang, J., Lapano, J., Keppens, V., Moore, R. G., Brahlek, M., Rost, C. M. & Ward, T. Z. "*Searching for superconductivity in high entropy oxide Ruddlesden–Popper cuprate films*". en. **Journal of Vacuum Science & Technology A 40,** 013–404. doi:10.1116/6.0001441. (06/11/2023) (Jan. 2022).

36. Jacobsen, H., Zaliznyak, I. A., Savici, A. T., Winn, B. L., Chang, S., Hücker, M., Gu, G. D. & Tranquada, J. M. "*Neutron scattering study of spin ordering and stripe pinning in superconducting La 1.93 Sr 0.07 CuO 4*". en. **Physical Review B 92,** 174–525. doi:10.1103/PhysRevB.92.174525. (06/06/2023) (Nov. 2015).

37. Christensen, T. S. "*High temperature superconductors in cryogenic environment*". B.Sc. Thesis (University of Copenhagen, Aug. 2021).

38. Deng, H., Dong, C., Chen, H., Wu, F., Jia, S. L., Shen, J. C. & Zhao, Z. X. "*Structural refinement of RE_2 ACu_2O_6 from powder X-ray diffraction data RE s La, Nd, A s Sr, Ca/*". en. **Physica C**, 285–293. doi:https://doi.org/10.1016/S0921-4534(98)00703-5. (1999).

39. Yamaguchi, Y., Yamauchi, H., Ohashi, M., Yamamoto, H., Shimoda, N., Kikuchi, M. & Syono, Y. "*Observation of the Antiferromagnetic Ordering in La $_2$ CuO $_4$*". **Japanese Journal of Applied Physics 26,** L447. doi:10.1143/JJAP.26.L447. (06/09/2023) (Apr. 1987).

40. Allgeier, C., Heise, J., Reith, W., Schilling, J. S. & Andres, K. "*Magnetization studies of the high temperature superconductors La2CuO4-y and YBa2Cu3O7-y under hydrostatic pressure*". **Physica C: Superconductivity 157,** 293–300. doi:https://doi.org/10.1016/0921-4534(89)90018-X. (1989).

41. Ramadhan, M. R., Adiperdana, B., Ramli, I., Sari, D. P., Putri, A. E., Wydiaiswari, U., Rozak, H., Zaharim, W. N., Manaf, A., Mohamed-Ibrahim, B. K. M. I., Sulaiman, S., Kawamata, T., Adachi, T., Koike, Y. & Watanabe, I. "*Estimation of the on-site Coulomb potential 1 and covalent state in La2CuO4 by muon spin rotation 2 and density functional theory calculations*". en. **Physical Review Research 4,** 033–044. doi:10.1103/PhysRevResearch.4.033044. (06/08/2023) (July 2022).

42. Dume, I. "*Palladium oxides could make better superconductors*". en-GB. June 2023. URL: https://physicsworld.com/palladium-oxides-could-make-better-superconductors/ (06/11/2023).

8 Appendix

8.1 Tables of chemical measurements

	Calculated	Measured
$La(NO_3)_3 \cdot 6H_2O$ [g]	0.6676	0.6668
$Sr(NO_3)_2$ [g]	0.0265	0.0265
$Cu(NO_3)_2 \cdot 3H_2O$ [g]	0.2013	0.2014
Sorbitol [g]	0.6025	0.6025
H_2O [ml]	12.9	12.92
Concentrated HNO_3 [ml]	1.5	1.5

Table 4: $(La_{0.925}Sr_{0.075})_2CuO_4$

	Calculated	Measured
$La(NO_3)_3 \cdot 6H_2O$ [g]	0.6676	0.6674
$Sr(NO_3)_2$ [g]	0.0529	0.0532
$Nd(NO_3)_3 \cdot 6H_2O$ [g]	0.6758	0.6757
$Cu(NO_3)_2 \cdot 3H_2O$ [g]	0.4027	0.4028
Sorbitol [g]	1.2050	1.2053
H_2O [ml]	25.8	25.87
Concentrated HNO_3 [ml]	3	3

Table 5: $(La_{0.4625}Sr_{0.075}Nd_{0.4625})_2CuO_4$

	Calculated	Measured
$La(NO_3)_3 \cdot 6H_2O$ [g]	0.4450	0.4453
$Sr(NO_3)_2$ [g]	0.0529	0.0527
$Nd(NO_3)_3 \cdot 6H_2O$ [g]	0.4505	0.4504
$Eu(NO_3)_3 \cdot xH_2O$ [g]	0.3473	0.3475
$Cu(NO_3)_2 \cdot 3H_2O$[g]	0.4027	0.4030
Sorbitol [g]	1.2050	1.2050
H_2O [ml]	25.8	25.83
Concentrated HNO_3 [ml]	3	3

Table 6: $(La_{0.3083}Sr_{0.075}Nd_{0.3083}Eu_{0.3083})_2CuO_4$

8.2 Python Code

```
import numpy as np
import pandas as pd

# Molecular Weight in g/mol
WLa = 433.01
WSr = 211.63
WCu = 241.60
WNd = 438.35
WEu = 337.98
WSm = 444.47
WSorb = 0.6025*2 # We need double the sorbitol

# How many moles (5 millimoles):
Mol = 5e-3

# Order of experiments
# LaSrCu, LaSrNdCu, LaSrNdEuCu, LaSrNdEuSmCu
# Knowing the product we want, we calculate the stochiometric amount:
LaP = np.array([0.925, 0.4625, 0.3083, 0.2312])*2*Mol/3
SrP = np.ones(4)*0.075*2*Mol/3
CuP = np.ones(4)*Mol/3
NdP = np.array([0, 0.4625, 0.3083, 0.2312])*2*Mol/3
EuP = np.array([0, 0, 0.3083, 0.2312])*2*Mol/3
SmP = np.array([0, 0, 0, 0.2312])*2*Mol/3

# mL
LH2O = np.ones(4)*12.9*2
LNO3 = np.ones(4)*1.5*2

#Prints the sum of the moles (should all be ca. Mol the variable):
print(LaP+SrP+CuP+NdP+EuP+SmP)

amounts = pd.DataFrame({'LaNO$_3$ [g]':LaP*WLa, 'SrNO$_3$ [g]':SrP*WSr, '
    CuNO$_3$ [g]':CuP*WCu, 'NdNO$_3$ [g]':NdP*WNd,'EuNO$_3$ [g]':EuP*WEu,'
    SmNO$_3$ [g]':SmP*WSm,'Sorbitol [g]':WSorb , 'H$_2$O [ml]':LH2O, 'HNO$_3$
     [ml]':LNO3}, index=['LaSrCu', 'LaSrNdCu', 'LaSrNdEuCu', 'LaSrNdEuSmCu'])

amounts
```

8.3 Comparison of KAC-1: First and second synthesis

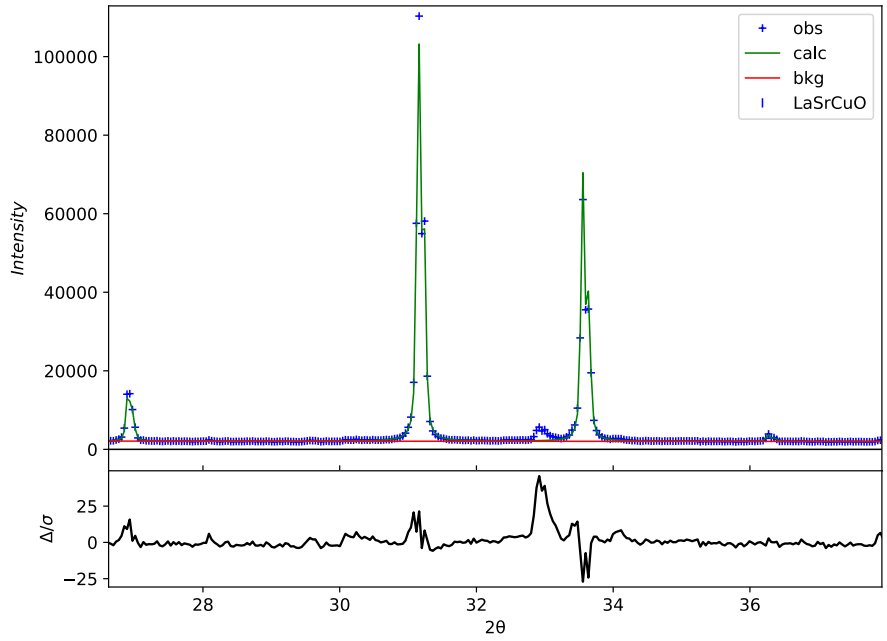

(a) First synthesis of KAC-1 with $La_{1.85}Sr_{0.15}CuO_4$ fitted.

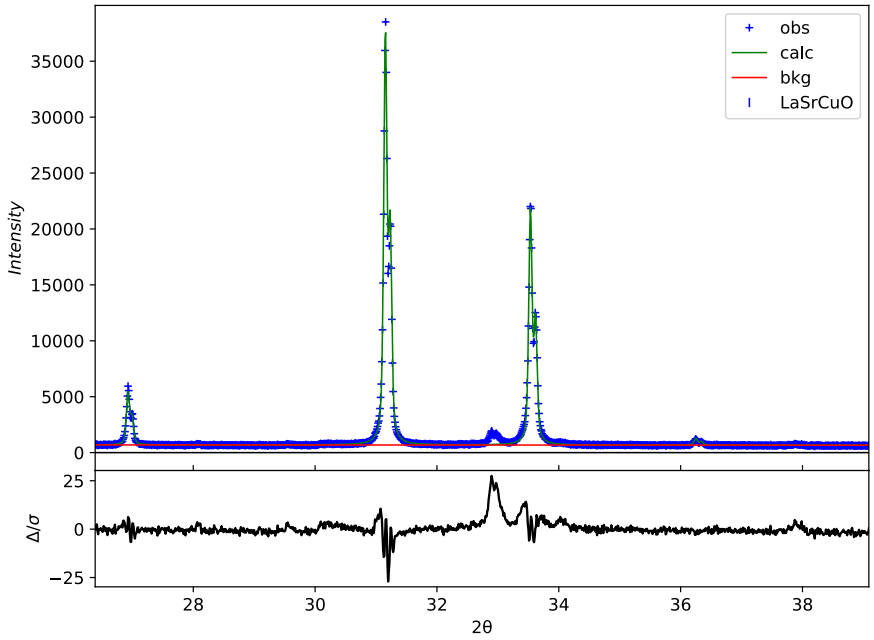

(b) Second synthesis of KAC-1 with $La_{1.85}Sr_{0.15}CuO_4$ fitted.